Far-infrared dielectric and vibrational properties of nonstoichiometric wüstite at high pressure

Christopher T. Seagle,[1,*] Wenxuan Zhang,[1] Dion L. Heinz,[1,2] and Zhenxian Liu[3]
[1]*Department of the Geophysical Sciences, University of Chicago, Chicago, Illinois 60637, USA*
[2]*James Franck Institute, University of Chicago, Chicago, Illinois 60637, USA*
[3]*Geophysical Laboratory, Carnegie Institution of Washington, Washington DC 20015, USA*
(Received 25 September 2008; revised manuscript received 19 November 2008; published 9 January 2009)

The far-infrared reflectivity of $Fe_{0.91}O$ was investigated from atmospheric pressure up to 33 GPa at room temperature using synchrotron Fourier transform infrared reflectivity techniques in conjunction with the diamond-anvil cell from 100–700 cm^{-1}. The frequency of the fundamental transverse optic (TO) mode was found to be nearly independent of pressure up to 4.6 GPa, followed by an increase in the TO frequency with pressure up to the rhombohedral phase transition at ~8 GPa. In addition, a second weak mode at 583 cm^{-1} at atmospheric pressure was well resolved and found to shift to higher frequency and increase in strength with pressure. This localized mode arises from the presence of vacancies in the crystal structure, and the relative strength of this mode suggests pressure-induced charge localization near the vacancy sites. The data was fit with the classical Lorentz model with the addition of a plasmon resonance. This allowed an estimation of the electrical conductivity as well as plasmon-phonon coupling energies. The pressure dependencies of the dielectric properties of wüstite have been quantified, and their pressure derivatives show a change in sign near the pressure-induced rhombohedral phase transition. Classical theories relating dielectric, vibrational, and elastic properties are evaluated, and in the case of the bulk modulus, the theory fails to reproduce accepted literature values.

DOI: 10.1103/PhysRevB.79.014104 PACS number(s): 78.20.Ci, 91.60.Mk, 63.20.Pw, 63.20.dd

I. INTRODUCTION

Wüstite, Fe_xO, is a vacancy ridden mineral that crystallizes in the rocksalt structure. It is a *p*-type semiconductor with a band gap of 2.3 eV.[1] Due to its geophysical and technological importance, wüstite has attracted a wealth of theoretical and experimental investigations into its vibrational, dielectric, and thermoelastic properties.[2–22] A pressure-induced rhombohedral distortion of the cubic lattice begins around 8–10 GPa depending on the degree of hydrostaticity.[15,23] Detailed theoretical investigations of wüstite often rely on comparison to thermoelastic data to corroborate their results. Here we present experimental data on the optical properties and vibrational modes at high pressure, which are more directly related to the band structure of wüstite and provide an additional set of constraints for theoretical band-structure studies.

When transversely polarized light interacts with a dielectric, phonons which induce atomic displacements that possess a nonzero dipole moment may be excited; these phonons are termed infrared (IR) active. The fundamental transverse optic mode is the only mode predicted to be IR active for diatomic materials that crystallize in the rocksalt structure. This phonon manifests as a peak in the reflectivity spectrum, and a careful analysis of the reflectivity can reveal detailed information on the dielectric and vibrational properties of the material.

The far-IR properties of wüstite have been investigated previously at atmospheric pressure,[3,19,24,25] although most of the data available in the literature is consistent, the interpretations tend to vary. In particular, the reflectivity is found to rise at low wavenumber, and there has been some disagreement as to whether this rise is instrumental in origin or intrinsic to wüstite.[24,25] Also, previous studies have ignored a small feature in the reflectivity spectrum, which we will suggest is related to vacancies in the crystal structure. An attempt is made to describe the origin of this mode and how its pressure dependence can give insights into how the local electronic structure changes with compression.

II. SAMPLE AND EXPERIMENT

The wüstite used for this experiment was Fe_xO with $x=0.91$ determined from powder x-ray diffraction measurements.[16] No other phases were detectable with x-ray diffraction suggesting the sample was nearly pure wüstite. The average grain size was ~100 μm. A symmetrical diamond-anvil cell was used with 500 μm culet diamonds of type Ia as a pressure generating device. A stainless-steel gasket was preindented to ~100 μm and a 400 μm hole was drilled in the center of the indentation to serve as the sample chamber. The sample chamber was packed with the wüstite and a single ruby ball (~5 μm diameter) was placed in the center of the sample chamber in contact with one of the diamond anvils. Position of the R1 ruby florescence line was used for pressure calibration.[26]

The infrared detector used was a liquid-helium-cooled bolometer. The synchrotron far-IR reflectivity experiments were preformed at the U2A beamline of the National Synchrotron Light Source (NSLS), Brookhaven National Laboratory. The IR light at the NSLS is a diffraction-limited source and ideal for reflectivity measurements at high pressure where the sample sizes are limited and the relatively thick diamond anvil acts as an absorber of radiation. However, the intensity of the IR radiation at the NSLS depends on the ring current and frequency. To overcome issues in data analysis caused by this problem the intensity of the light source must be calibrated as a function of frequency and ring

current. This is accomplished by repeatedly measuring the intensity of light reflected off of the back plate of one of the diamond anvils. The optical properties of the diamond are of course independent of the ring current so these measurements provide a means to correct the reflected intensity measured off of any interface to any ring current. These reference spectra are crucial to obtaining accurate reflectivity values.

Four measurements in addition to the current correction are required to calculate the reflectivity of the diamond-sample interface, R_d. These consist of: the power reflected off of the air-gold interface, I_0; the power reflected off of the air-diamond interface, $I_{\text{diamond}}=I_0R_{\text{diamond}}$, where R_{diamond} is the reflectivity of diamond; the power reflected off of the diamond-air interface (through the diamond), $I_e=I_0R_{\text{diamond}}(1\text{-}R_{\text{diamond}})^2(1\text{-}A_{\text{diamond}})^2$, where A_{diamond} is the absorbtivity of diamond; and the power reflected off of the diamond-sample interface, $I_s=I_0R_d(1\text{-}R_{\text{diamond}})^2(1\text{-}A_{\text{diamond}})^2$. Combination of the above relations yields a formula for the reflectivity of the diamond-sample interface

$$R_d=\frac{I_s}{I_e}\frac{I_{\text{diamond}}}{I_0}. \tag{1}$$

Equation (1) assumes that the reflectivity of gold is close to one throughout the measured frequency range, and it does not account for possible back reflections or the possible pressure dependence of diamond absorption. I_0 and I_e were measured once before the sample was loaded; I_{diamond} and I_s were measured for each pressure point.

III. DATA ANALYSIS

A classical dispersion analysis was preformed to extract the optical constants as a function of pressure and frequency. The reflectivity data and the corresponding fits to that data are shown in Fig. 1. There has been some debate as to the nature of the rise of the reflectivity in the low-frequency region. In this analysis we have assumed that because wüstite is a semiconductor with finite dc conductivity that the rise in the reflectivity as the frequency tends to zero is intrinsic behavior of the sample. In fact, all previous data at atmospheric pressure[3,19] have shown a similar rise at low frequency, and one study at low temperatures showed that this behavior disappears as temperature is decreased as would be expected for a semiconductor.[24] The index of refraction of magnesiowüstites has been measured optically at atmospheric pressure up to 66.7 mol % FeO, and found to follow a linear trend.[27] An extrapolation of this trend to pure FeO suggests an index of refraction of 2.32 in the visible. However, taking $\varepsilon_\infty=n^2$ for the atmospheric pressure data produces a very poor fit, therefore ε_∞ was treated as a free parameter and the best fit produced $\varepsilon_\infty=11.73(1)$, suggesting an index of refraction of ~3.43 in the visible. This is significantly higher than the extrapolation of optically measured indices of refraction for magnesiowüstites, but it may not be unreasonable as the transition from transparent to opaque is likely accompanied by a steep rise in the index of refraction.

At atmospheric pressure a very weak peak in the reflectivity spectrum is present at 583 cm^{-1}, this peak has been observed by other authors,[3,19,24] and was found to decrease in intensity as temperature was lowered.[24] This peak was ignored in previous quantitative analysis of the data because of its very weak strength and unknown origin. Consistent with previous work, this peak was observed; it was found to increase in intensity with increasing pressure. The origin of this peak will be discussed below. We treated the dielectric function to be a sum of two oscillators plus a plasmon resonance, except for the highest pressure point at 33 GPa where the second weak peak in the reflectivity spectrum has slipped beyond the frequency range of this study. We assume a dielectric function of the form below, where the summation goes only to one for the 33 GPa data,

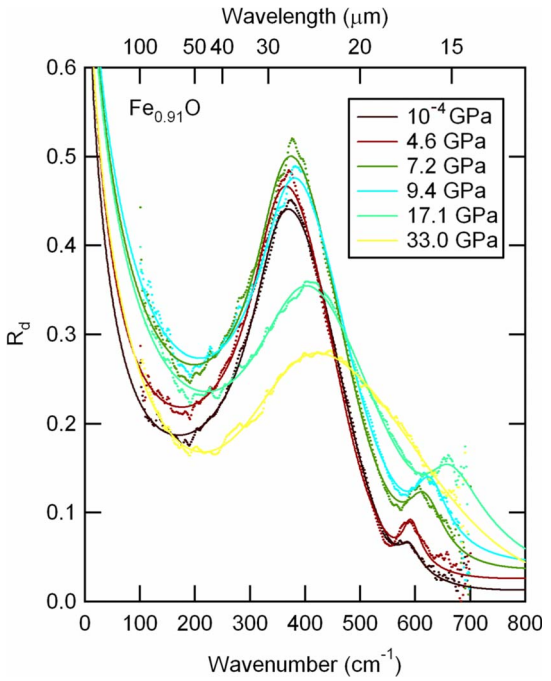

FIG. 1. (Color online) Reflectivity of the diamond-wüstite interface at various pressures. The dots are the raw data; the solid lines are the best fits of those data to Eq. (4).

$$\hat{\varepsilon}(\omega)=\varepsilon_1+i\varepsilon_2=\varepsilon_\infty-\frac{\varepsilon_\infty\omega_p^2}{\omega^2+i\gamma_p\omega}+\sum_{j=1}^{2}\frac{f_j\omega_j^2}{\omega_j^2-\omega^2-i\gamma_j\omega}, \tag{2}$$

where ε_1 and ε_2 are the real and imaginary parts of the dielectric function, respectively, ε_∞ is the background dielectric constant, ω_p is the plasma frequency, γ_p is the plasma damping factor, f_j, ω_j, and γ_j are the strength, frequency, and damping factor of oscillator j, respectively. Prévot *et al.*[19] used an identical form as this with only one oscillator plus the plasmon resonance. The complex index of refraction is defined as $\hat{N}=n+ik$, in the case of diamond the extinction coefficient, k, is much less than one and therefore $\hat{N}_{\text{diamond}}=n_d$. The index of refraction, n, and the extinction coefficient, k, are related to the real and imaginary parts of the dielectric function through the relations $\varepsilon_1=(n^2-k^2)/\mu$ and $\varepsilon_2=2nk/\mu$, where μ is the permeability. The reflectivity of the diamond-sample interface is given by

TABLE I. Best fit to Eq. (4), all values in cm^{-1}, except pressure (GPa).

Pressure (GPa)	10^{-4}	4.6	7.2	9.4	17.1	33.0
ε_∞	12.7 ± 0.1	15.0 ± 0.2	18.1 ± 0.2	18.1 ± 0.3	11.8 ± 0.3	7.1 ± 0.1
ν_p	469 ± 21	570 ± 52	565 ± 34	660 ± 50	851 ± 21	525 ± 20
γ_p	1073 ± 105	1470 ± 279	1078 ± 137	1342 ± 205	1756 ± 235	631 ± 50
ν_1	335.2 ± 0.6	335.4 ± 0.8	345 ± 1	354 ± 1	373.5 ± 0.5	357 ± 2
γ_1	86.3 ± 0.6	81.6 ± 0.8	83 ± 1	93 ± 1	155 ± 1	202 ± 2
f_1	14.2 ± 0.1	16.0 ± 0.1	18.6 ± 0.2	18.0 ± 0.2	14.3 ± 0.1	10.3 ± 0.2
ν_2	583 ± 2	588 ± 1	610 ± 2	620 ± 2	649 ± 2	
γ_2	41 ± 6	37 ± 5	71 ± 9	65 ± 8	99 ± 7	
f_2	0.10 ± 0.01	0.19 ± 0.02	0.46 ± 0.07	0.46 ± 0.06	0.55 ± 0.05	

$$R_d = \left| \frac{\hat{N}_{\text{diamond}} - \hat{N}_{\text{sample}}}{\hat{N}_{\text{diamond}} + \hat{N}_{\text{sample}}} \right|^2. \quad (3)$$

Combining the relations above leads to the following formula for the reflectivity of the diamond-sample interface in terms of the index of refraction of diamond, and the dielectric function of the sample:

$$R_d = \frac{n_d^2 + \sqrt{\varepsilon_1^2 + \varepsilon_2^2} - \sqrt{2} n_d (\varepsilon_1 + \sqrt{\varepsilon_1^2 + \varepsilon_2^2})^{1/2}}{n_d^2 + \sqrt{\varepsilon_1^2 + \varepsilon_2^2} + \sqrt{2} n_d (\varepsilon_1 + \sqrt{\varepsilon_1^2 + \varepsilon_2^2})^{1/2}}, \quad (4)$$

n_d is approximately constant over the far IR; and we have taken the permeability to be one. The particular diamond used in this study had a nearly constant reflectivity of 17.7% from 100–700 cm^{-1} corresponding to an index of refraction of 2.4554.

A nonlinear regression was preformed for Eq. (4) beginning with the values of the plasmon and phonon constants given by Prévot *et al.*,[19] the phonon parameters corresponding to the second peak in the reflectivity spectrum were initially guessed. The regression at each successive pressure was started at values obtained at the previous pressure. The results of these regressions are presented schematically in Fig. 1 and the values of the plasmon and phonon parameters are tabulated in Table I. No interference fringes are apparent in the raw data, suggesting that it was not necessary to account for back reflections from the sample in Eq. (1). The dielectric functions are presented in Fig. 2, and the corresponding complex index of refraction is presented in Fig. 3. The maximum value of the vacuum-wüstite reflectivity at atmospheric pressure derived from the fit is 70%, compared to 70,[24] 66,[19] and ~75%.[3] The good agreement with the magnitude of the maximum reflectivity, shape, and presence of the second weak peak in the reflectivity spectrum all indicate that the data collected in this study is accurate. Various other optical properties such as the optical conductivity and surface impedance are related to the dielectric function and may be calculated as a function of pressure and frequency with the data presented in Table I.

The main peak in the reflectivity spectrum of wüstite is due to the transverse-optic (TO) vibrational mode. The TO modes are given by the poles of the dielectric function minus the plasmon resonance, and the longitudinal-optic (LO) modes are given by the zeros. An interaction with the plasmon resonance and optic modes results in two additional branches caused by plasmon-phonon coupling, which may

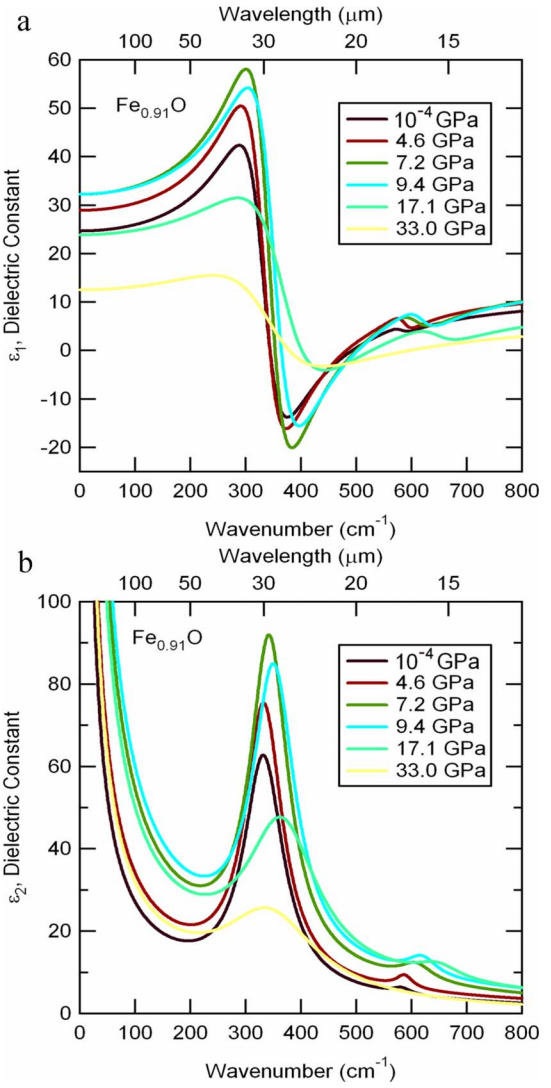

FIG. 2. (Color online) (a) Real and (b) imaginary parts of the dielectric function of $Fe_{0.91}O$ at various pressures.

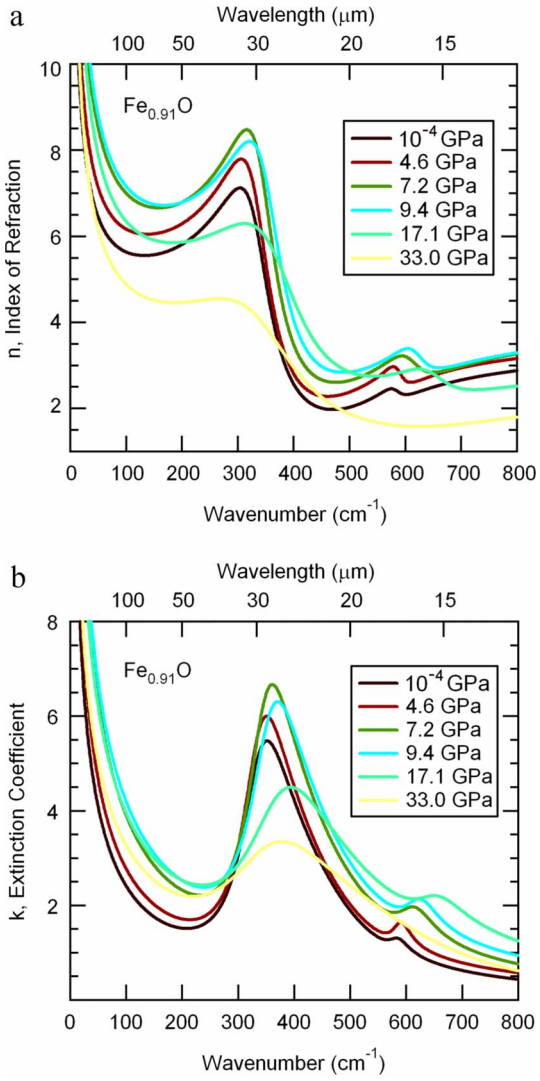

FIG. 3. (Color online) (a) Real and (b) imaginary parts of the index of refraction of $Fe_{0.91}O$ at various pressures.

take on complex values depending on the relative magnitude of the plasma frequency and the TO frequency. These frequencies are known as ν_+ and ν_-, in this study the real part of ν_+ is nonzero and has a value of 507 ± 3 cm^{-1} at atmospheric pressure, compared to 508 cm^{-1} from reflectivity measurements[19] and 527 ± 13 cm^{-1} from neutrons.[14] The presence of this mode is reflected in the broadening of the main peak in the reflectivity spectrum. Semiconductors which do not possess a finite dc conductivity typically have very sharp drops in the magnitude of their reflectivity at frequencies higher than the frequency of the TO mode. The frequency of the modes determined from the zeros and poles of the dielectric function and their dominant character are presented in Table II.

Origin of the 583 cm^{-1} mode

Previous studies on the reflectivity of nonstoichiometric wüstite at atmospheric pressure have revealed a small feature near 583 cm^{-1}. This mode was not treated in detail previously because it has very small strength compared to the TO mode and its origin was not understood. Indeed, if only the atmospheric pressure data in Fig. 1 were examined it would be easy to ignore this feature. However, this peak shifts position and increases in strength with increasing pressure, strongly suggesting that the origin of this mode is related to the phonon dynamics of wüstite and is not the result of experimental artifact. There have been many theoretical investigations into the normal modes of linear diatomic chains, and the effects that vacancies and mass defects have on the frequency of those modes and their IR strengths.[28]

We have developed a very simple model using a linear chain of alternating Fe and O atoms in which every tenth iron atom is missing (corresponding to $Fe_{0.9}O$) where nearest-neighbor interactions occur. The spring constant, k, is identical for all atom pairs except those nearest the vacancy where we allow the spring constant to vary, this constant is k'. The free oscillations of a 19-atom chain with periodic boundary conditions were solved with *Mathematica*. This is shown schematically in Fig. 4(a). Following the method of Barker and Sievers,[28] we solve for the normal-mode frequencies and IR strengths; we find that the frequency of the TO mode depends only on the atomic masses and the spring constant k. The atomic displacements for the TO mode are presented in Fig. 4(b). The presence of vacancies in the lattice give rise to a new mode termed the localized mode, in which atoms near the vacancy oscillate with large amplitude. In this model the frequency of this mode is doubly degenerate and the sum of the two eigenvectors corresponding to this mode was summed to produce Fig. 4(c). The values of the spring constants k, and k', where chosen such that the observed TO and localized mode frequencies were reproduced by the model at atmospheric pressure.

It should be noted that for most systems, introduction of a vacancy is usually expected to induce softening of the bonds of the nearest neighbors. This will give rise to a gap mode whose frequency falls between the optic and acoustic

TABLE II. Calculated phonon, and plasmon-phonon coupling frequencies in cm^{-1} derived from the dielectric function, Eq. (3) (see text for details).

	Pressure (GPa)					
Mode character	10^{-4}	4.6	7.2	9.4	17.1	33.0
TO	332.4(6)	332.9(8)	343(1)	351(1)	365.4(5)	343(2)
LO	486(2)	481(4)	490(4)	497(5)	551(8)	551(7)
Localized mode	583(2)	588(1)	609(2)	619(2)	647(2)	
ν_+	507(3)	491(7)	512(9)	507(11)	558(17)	665(7)

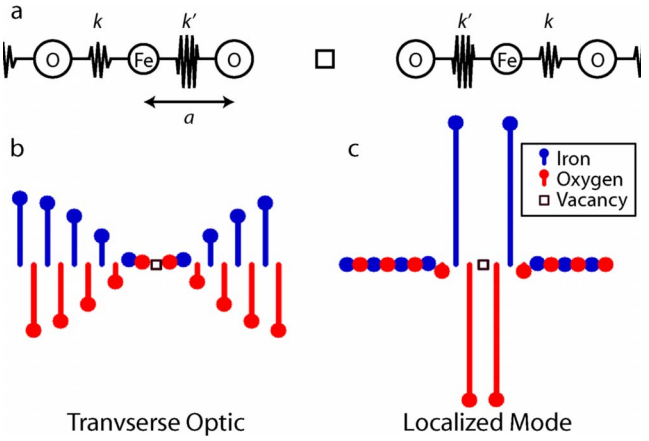

FIG. 4. (Color online) (a) Spring model for nonstoichiometric wüstite; [(b) and (c)] atomic displacements plotted in the vertical direction for the two strongest normal-mode frequencies of a 19-atom iron oxide chain with one iron vacancy ($Fe_{0.9}O$). Atomic displacements are exaggerated relative to atomic spacing, the displacements for the TO and localized modes are plotted on the same scale.

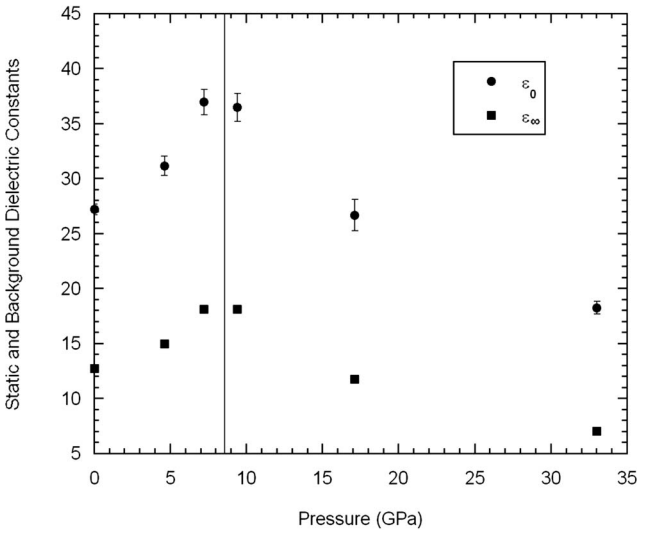

FIG. 5. Static, ε_0, and background, ε_∞, dielectric constants as a function of pressure. The vertical line shows the approximate structural transition pressure from rocksalt to rhombohedral under nonhydrostatic conditions. Estimated errors on ε_∞ are smaller than the symbols.

branches.[29] Localized modes such as the one observed here are theoretically possible only when some relaxation of the atomic positions around the vacancy occurs.[30] In the spring model presented here the bond distances were assumed to be uniform throughout the lattice, and therefore it is only meant to provide a very rough description of the vibrational modes. A detailed three-dimensional model taking account of all force constants which reproduce the vibrational density of states and elastic constants would certainly provide more insights into the details regarding the origin of this mode.

The relative infrared strengths of the modes in the spring model are related to the frequencies of the modes and the net dipole moments induced by the atomic displacements. The ratio of the IR strengths of the TO and localized modes are approximately given by

$$\frac{f_{\mathrm{TO}}}{f_{\mathrm{local}}} = \left(\frac{z_{\mathrm{TO}}\nu_{\mathrm{local}}}{z_{\mathrm{local}}\nu_{\mathrm{TO}}}\right)^2, \tag{5}$$

where z is the net induced dipole moment, assuming that the density of vacancies remains constant. The frequencies and strengths of these modes have been measured as a function of pressure, and therefore it is possible to extract information on changes in charge distribution around the vacancies. When an Fe^{2+} is removed from the ideal lattice and replaced with a vacancy, a charge deficit occurs and the charge on the lattice must be balanced by the addition of two electrons. Whether this occurs as a definite site on the lattice going from Fe^{2+} to Fe^{3+} or if these extra charges are distributed in some way among the remaining iron atoms is not well understood, however it is possible to make some speculations based on Eq. (5).

Inspection of Figs. 2(b) and 2(c) shows that the net dipole moment induced by atomic displacements for the localized mode will be maximized when the iron atoms nearest the vacancy take on the extra charge lost by inclusion of the vacancy, while the net dipole moment of the transverse optic mode is essentially unaffected because the motions of the iron atoms near the vacancy is small compared to iron atoms far from the vacancy. Hence, balancing charge by placing Fe^{3+} ions on the iron sites nearest the vacancy will minimize the ratio $z_{\mathrm{TO}}/z_{\mathrm{local}}$, and placing Fe^{3+} ions on iron sites far from the vacancy will maximize $z_{\mathrm{TO}}/z_{\mathrm{local}}$. Applying Eq. (5) to the data in Table I indicates that $z_{\mathrm{TO}}/z_{\mathrm{local}}$ decreases nearly linearly from 6.8 ± 0.5 at 10^{-4} GPa to 2.9 ± 0.1 at 17 GPa. A quantitative treatment of the charge distribution is not possible using the simple one-dimensional model of the solid; however the trend in the data would suggest that as pressure increases, the extra charges are increasingly concentrated closer to the vacancy sites. This is also reflected in the ratio of the spring constants, k'/k. In the model this ratio gets larger with increasing pressure in order to match the observed TO and localized mode frequencies; the bonds near the vacancy get stronger as the additional electrons needed for charge balance tend to spend more time around the atoms near the vacancy as pressure increases.

IV. DERIVED PROPERTIES

The Lyddane-Sachs-Teller (LST) relation links the IR frequencies of the crystal to the ratio of the static and background dielectric constants[31]

$$\frac{\varepsilon_0}{\varepsilon_\infty} = \left(\frac{\nu_{\mathrm{LO}}}{\nu_{\mathrm{TO}}}\right)^2. \tag{6}$$

The static dielectric constant, ε_0, determined from this relation at atmospheric pressure is 27.2 ± 0.5, where we have used only the main TO and LO modes, compared to a value of 24 determined from a previous reflectivity study at 10^{-4} GPa.[19] The value of ε_0 calculated from Eq. (6) is presented in Fig. 5. There is clearly a change in behavior asso-

ciated with the rocksalt to rhombohedral structural phase transition.

The Lorentz-Lorenz formula relates the background dielectric constant, ε_∞, with the electronic polarizability, α_∞

$$\alpha_\infty = \frac{3V}{4\pi}\left(\frac{\varepsilon_\infty - 1}{\varepsilon_\infty + 2}\right), \tag{7}$$

where V is the volume per ion pair. Application of Eq. (7) gives the electronic polarizability at atmospheric pressure to be 3.76 ± 0.04 Å^3. This is in fair agreement with a previous study,[19] 3.62 Å^3, and the relatively high value reflects the large effective volume of oxygen in the lattice. A similar formula, the Clausius-Mossotti relation, connects the static dielectric constant, ε_0, with the static polarizability, α_0

$$\alpha_0 = \frac{3V}{4\pi}\left(\frac{\varepsilon_0 - 1}{\varepsilon_0 + 2}\right). \tag{8}$$

Application of Eq. (8) at atmospheric pressure results in a static polarizability of 4.1 ± 0.1 Å^3, in good agreement with the value of 4.2 Å^3, based on the data of Prévot *et al.*[19]

In the limit of zero frequency, the real part of the optical conductivity reduces to the dc conductivity; hence, the dc conductivity is related to the plasmon parameters determined in the fit of the data to Eq. (4)

$$\sigma_{\mathrm{dc}} = \frac{\varepsilon_\infty \nu_p^2}{60\gamma_p}(\Omega^{-1}\ \mathrm{cm}^{-1}), \tag{9}$$

where ν_p, and γ_p are expressed in cm^{-1}. Equation (9) suggests a dc conductivity of 44 ± 6 Ω^{-1} cm^{-1} at atmospheric pressure. This value is a factor of ~2.5 larger than that determined in a previous reflectivity study,[19] and ~4.4 times larger than the dc conductivity determined from direct electrical measurements.[3] Differences in the position of the upturn in the reflectivity spectrum as the frequency tends to zero results in the difference in the magnitude of the dc conductivity determined here at that of Prévot *et al.*[19] and may be due to difference in stoichiometry between the two samples. We note that the dc conductivity derived from reflectance measurements often deviates from direct electrical measurements even in the case of metals.[32] The electrical conductivity of wüstite depends on the nonstoichiometry and is found to increase with decreasing x in Fe_xO.[33] The arrangement of vacancies in wüstite is not random,[34] and it is likely that the density and agglomeration of defects play a critical role in the origin and magnitude of the electrical conductivity.[6] The magnitude of the dc conductivity derived from the reflectivity measurements initially rises with pressure before reaching a maximum and then decreasing. There are two competing effects that contribute to the magnitude of the dc conductivity. First is the mobility of vacancies through the lattice which to first order scales with bond strength. Second is the charge associated with the vacancies. We have provided evidence that, upon compression, charge is concentrated near the vacancy sites, this likely leads to the rise in the conductivity at low pressure. However, the vacancy mobility decreases with pressure as the density rises and the bonds near the vacancies become stronger. This effect begins to dominate between 9.4 and 17.1 GPa, causing a decrease in the dc conductivity.

The first Szigeti relation[35] in the classical theory of dielectric polarization relates the incompressibility of the lattice to the frequency of the transverse optic mode

$$K = \left(\frac{\varepsilon_0 + 2}{\varepsilon_\infty + 2}\right)\frac{\mu\omega_{\mathrm{TO}}^2}{3V^{1/3}}, \tag{10}$$

where K is the bulk modulus, μ is the reduced mass of an ion pair, and V is the volume per ion pair. Equation (10) is strictly valid only at zero pressure. Barron and Batana,[36] generalized the first Szigeti relation to any pressure and obtained the following, presented here in slightly different form valid for the rocksalt structure

$$K = \left(\frac{\varepsilon_0 + 2}{\varepsilon_\infty + 2}\right)\frac{\mu\omega_{\mathrm{TO}}^2}{3V^{1/3}} + \frac{4}{3}P, \tag{11}$$

where P is the pressure. The volume of our wüstite sample was measured at atmospheric pressure by x-ray diffraction to be 79.06(6) Å^3 per unit cell. Using Eqs. (10) and (11) we obtained $K = 125 \pm 4$ GPa for the zero-pressure bulk modulus. Literature values for the zero-pressure bulk modulus of wüstite determined experimentally range from 142 ± 10 GPa,[37] for $Fe_{0.907}O$ up to 174 ± 12 GPa,[17] for $Fe_{0.98}O$. The value of the zero-pressure bulk modulus determined from this dielectric data at atmospheric pressure is significantly lower than all theoretical, ultrasonic, and compression studies, suggesting a breakdown of the classical theory for wüstite. The specific volume of the wüstite sample was not measured at high pressure so significant uncertainty exists as to the volume of the sample at high pressure; however if we adopt the equation of state for $Fe_{0.907}O$ measured by x-ray diffraction compression studies,[37] we can use Eq. (11) to calculate the bulk modulus expected based on the classical theory. We note that the volume dependence of the bulk modulus in this theory is relatively weak, and therefore the choice of the equation of state to calculate the volume of the wüstite as a function of pressure does not have a significant effect on the calculated bulk modulus according to Eq. (11). The first pressure derivative of the bulk modulus between 4.6 and 9.4 GPa determined from these calculations is ~4. The bulk modulus appears to increase much more slowly during the rhombohedral distortion of the lattice consistent with significant softening of the C_{44} elastic constant.[23]

The second Szigeti relation,[38] in the classical theory correlates the effective charge of the ions to the frequency of the transverse-optic mode

$$e_s^* = \left[\frac{9V\mu\omega_{\mathrm{TO}}^2}{4\pi}\left(\frac{\varepsilon_0 - \varepsilon_\infty}{(\varepsilon_\infty + 2)^2}\right)\right]^{1/2}. \tag{12}$$

For a purely ionic Fe-O bond, the Szigeti effective charge, e_s^*, should be 2 since this is the valence state of both Fe and O. However, since the bond is not completely ionic, and some Fe^{3+} must be present in the lattice to maintain charge balance, the effective charge may be altered from its ideal value. Indeed for most materials the Szigeti effective charge is found to be much lower than its ideal value,[39] and the value found at 10^{-4} GPa here, $(0.57 \pm 0.02)e$, is in good

TABLE III. Calculated properties of wüstite, the static dielectric constant, ε_0; static polarizability, α_0; electric polarizability, α_∞; electrical conductivity, σ; Szigeti effective charge, e_s^* (ratio to electron charge); and bulk modulus, K; see text for details.

Pressure (GPa)	10^{-4}	4.6	7.2	9.4	17.1	33.0
ε_0	27.2 ± 0.5	31.2 ± 0.9	37 ± 1	36 ± 1	27 ± 1	18.3 ± 0.6
α_0 (Å^3)	4.2 ± 0.1	4.2 ± 0.2	4.1 ± 0.2	4.1 ± 0.2	3.8 ± 0.3	3.4 ± 0.2
α_∞ (Å^3)	3.76 ± 0.04	3.76 ± 0.07	3.82 ± 0.07	3.77 ± 0.08	3.3 ± 0.1	2.65 ± 0.07
σ (Ω^{-1} cm^{-1})	44 ± 6	55 ± 15	89 ± 16	98 ± 21	81 ± 16	52 ± 6
e_s^*/e	0.57 ± 0.02	0.52 ± 0.03	0.48 ± 0.03	0.48 ± 0.03	0.65 ± 0.06	0.77 ± 0.04
K (GPa)	124 ± 4	131 ± 7	141 ± 9	149 ± 10	187 ± 18	202 ± 11

agreement with a previous study,[19] $0.62e$. The Szigeti effective charge first decreases with pressure up to the rhombohedral transition where it begins to increase with further compression. A summary of the derived properties of wüstite is presented in Table III.

The optic mode Grüneisen parameters are defined as

$$\gamma_j = -\frac{\partial(\ln \nu_j)}{\partial(\ln V)}. \tag{13}$$

In Fig. 6 we have plotted the mode frequencies as a function of volume adopting the equation of state of $Fe_{0.908}O$.[37] As can be seen in the figure wüstite exhibits rather unusual behavior up to 4.6 GPa. Below this pressure, the frequencies of the TO and LO modes have a slope of nearly zero or negative, respectively. It is likely that this observation is related to the vacancies in wüstite. Going back to the spring model, the TO frequency is independent of the force constant k', while the localized mode frequency depends on both k and k'. The frequency of the localized mode does slightly increase with pressure in the 0–4.6 GPa range, suggesting that if k is constant then k' must be increasing. This is indeed what is found in the model and it suggests that most of the compression taking place is initially concentrated around the vacancy sites. The simple spring model cannot quantify this effect because the initial assumption was that the spacing between all sites are the same; however it does show that it is at least plausible that the pressure independence of the TO and LO frequencies below 4.6 GPa could be related to the unusually large density of vacancies in $Fe_{0.91}O$. Above 17 GPa, the TO and LO mode frequencies show softening. In the 33 GPa data the frequency of the localized mode has slipped beyond the measured frequency range, and thus the data was only fit to one phonon plus the plasmon resonance. However, if the localized mode parameters are prescribed in Eq. (4) based on an extrapolation of the lower pressure data, there is almost no effect on the TO mode parameters or the plasmon parameters. This would suggest that the softening observed is an intrinsic property of wüstite.

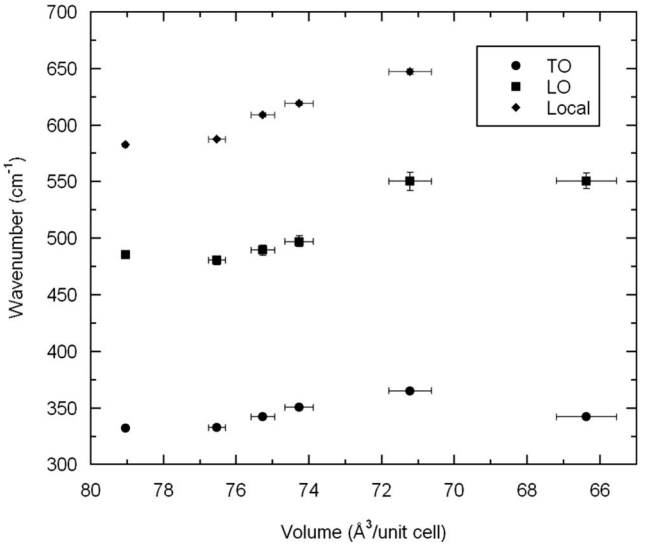

FIG. 6. Optic and localized mode frequencies of $Fe_{0.91}O$ plotted against unit-cell volume. See text for details.

Most materials do not have such a large concentration of vacancies, and therefore we may expect that simple averaging of the optic mode frequencies to estimate the thermal Grüneisen parameter is probably not applicable in the case of wüstite, although these averages seem to be reasonably good for many materials.[40,41] The optic mode Grüneisen parameters for the TO and LO modes are ~0 below 4.6 GPa. At higher pressures the rhombohedral distortion of the lattice becomes significant and also appears to play a role in the frequencies of the optic modes. As is evident from Fig. 5, this distortion begins to have an effect on the optical properties around 8 GPa; however the frequencies of all three modes vary approximately linearly with pressure between 4.6 and 9.4 GPa, indicating it may be useful to define an average Grüneisen parameter for the observed modes in this pressure range. A linear regression of the data in this pressure range leads to the following Grüneisen parameters: $\gamma_{TO} = 1.756 \pm 0.007$, $\gamma_{LO} = 1.14 \pm 0.01$, and $\gamma_{Local} = 1.8 \pm 0.3$. Application of the averaging of the TO and LO mode Grüneisen parameters results in an estimate of the thermal Grüneisen parameter, $\gamma_{Thermal} = 1.34 \pm 0.02$. This value seems reasonable; however the issues described above clearly raise questions about the accuracy of the thermal Grüneisen parameter derived in this manner.

V. CONCLUSIONS

Synchrotron far-IR reflectivity measurements have been performed on $Fe_{0.91}O$ up to a pressure of 33 GPa at room temperature. The frequencies of the TO and LO modes ap-

pears to be nearly independent of pressure up to 4.6 GPa, suggesting that most of the compression initially takes place around the vacancy sites. A second peak in the reflectivity spectrum was observed at higher wavenumber than the TO mode. The origin of this mode is suggested to be associated with large amplitude vibrations of the nearest neighbors of vacancies, and a simple spring model was developed to illustrate the origin of this mode. The strength of this mode increases with pressure, suggesting that the extra charges required for charge balance when introducing a vacancy tend to increasingly concentrate close to the vacancy sites. The static and background dielectric constants of wüstite show a change in the sign of their pressure derivatives very close to the pressure that the rhombohedral distortion of the cubic lattice is expected to occur. Finally, classically theories based on electronic polarizability that relate dielectric, vibrational, and elastic properties fail to satisfactorily reproduce the bulk modulus of wüstite.

ACKNOWLEDGMENTS

We thank two anonymous reviewers for their helpful comments. This work was partially supported by DOE-NNSA(CDAC). This research was partially supported by COMPRES, the Consortium of Materials Properties Research in Earth Sciences under NSF Cooperative Agreement No. EAR 06-49658. Use of the National Synchrotron Light Source, Brookhaven National Laboratory, was supported by the U.S. Department of Energy, Office of Science, Office of Basic Energy Sciences, under Contract No. DE-AC02-98CH10886.

*Corresponding author.

[1] J. M. Honig, Proc.-Indian Acad. Sci., Chem. Sci. **96**, 391 (1986).
[2] J. Badro, V. V. Struzhkin, J. F. Shu, R. J. Hemley, H. K. Mao, C. C. Kao, J. P. Rueff, and G. Y. Shen, Phys. Rev. Lett. **83**, 4101 (1999).
[3] H. K. Bowen, D. Adler, and B. H. Auker, J. Solid State Chem. **12**, 355 (1975).
[4] Y. Ding, J. Xu, C. T. Prewitt, R. J. Hemley, H. K. Mao, J. A. Cowan, J. Z. Zhang, J. Qian, S. C. Vogel, K. Lokshin, and Y. S. Zhao, Appl. Phys. Lett. **86**, 052505 (2005).
[5] Y. W. Fei and H. K. Mao, Science **266**, 1678 (1994).
[6] E. Gartstein, J. B. Cohen, and T. O. Mason, J. Phys. Chem. Solids **47**, 775 (1986).
[7] S. A. Gramsch, R. E. Cohen, and S. Y. Savrasov, Am. Mineral. **88**, 257 (2003).
[8] D. G. Isaak, R. E. Cohen, M. J. Mehl, and D. J. Singh, Phys. Rev. B **47**, 7720 (1993).
[9] R. Jeanloz and T. J. Ahrens, Geophys. J. R. Astron. Soc. **62**, 505 (1980).
[10] A. P. Kantor, L. S. Dubrovinsky, N. A. Dubrovinskaia, I. Y. Kantor, and I. N. Goncharenko, J. Alloys Compd. **402**, 42 (2005).
[11] A. P. Kantor, S. D. Jacobsen, I. Y. Kantor, L. S. Dubrovinsky, C. A. McCammon, H. J. Reichmann, and I. N. Goncharenko, Phys. Rev. Lett. **93**, 215502 (2004).
[12] E. Knittle and R. Jeanloz, Geophys. Res. Lett. **13**, 1541 (1986).
[13] E. Knittle and R. Jeanloz, J. Geophys. Res. Solid Earth **96**, 16169 (1991).
[14] G. Kugel, C. Carabatos, B. Hennion, B. Prevot, A. Revcolevschi, and D. Tocchetti, Phys. Rev. B **16**, 378 (1977).
[15] H. K. Mao, J. F. Shu, Y. W. Fei, J. Z. Hu, and R. J. Hemley, Phys. Earth Planet. Inter. **96**, 135 (1996).
[16] C. A. McCammon and L.-g. Liu, Phys. Chem. Miner. **10**, 106 (1984).
[17] H. Mizutani, S. Akimoto, and O. Nishizaw, Trans. Am. Geophys. Union **53**, 527 (1972).
[18] M. Murakami, K. Hirose, S. Ono, T. Tsuchiya, M. Isshiki, and T. Watanuki, Phys. Earth Planet. Inter. **146**, 273 (2004).
[19] B. Prevot, J. Biellmann, M. F. Meftah, and M. Sieskind, Phys. Status Solidi A **40**, 503 (1977).
[20] C. T. Seagle, D. L. Heinz, A. J. Campbell, V. B. Prakapenka, and S. T. Wanless, Earth Planet. Sci. Lett. **265**, 655 (2008).
[21] V. V. Struzhkin, H. K. Mao, J. Z. Hu, M. Schwoerer-Bohning, J. F. Shu, R. J. Hemley, W. Sturhahn, M. Y. Hu, E. E. Alp, P. Eng, and G. Y. Shen, Phys. Rev. Lett. **87**, 255501 (2001).
[22] J. Z. Zhang and Y. S. Zhao, Phys. Chem. Miner. **32**, 241 (2005).
[23] W. Mao, J. F. Shu, J. Z. Hu, R. Hemley, and H. Mao, J. Phys.: Condens. Matter **14**, 11349 (2002).
[24] T. Henning and H. Mutschke, Astron. Astrophys. **327**, 743 (1997).
[25] A. M. Hofmeister, E. Keppel, and A. K. Speck, Mon. Not. R. Astron. Soc. **345**, 16 (2003).
[26] I. F. Silvera, A. D. Chijioke, W. J. Nellis, A. Soldatov, and J. Tempere, Phys. Status Solidi B **244**, 460 (2007).
[27] N. L. Bowen and J. F. Schairer, Am. J. Sci. **29**, 151 (1935).
[28] A. S. Barker, Jr. and A. J. Sievers, Rev. Mod. Phys. **47**, S1 (1975).
[29] Y. Mitani and S. Takeno, Prog. Theor. Phys. **33**, 779 (1965).
[30] P. L. Land and B. Goodman, J. Phys. Chem. Solids **28**, 113 (1967).
[31] R. H. Lyddane, R. G. Sachs, and E. Teller, Phys. Rev. **59**, 673 (1941).
[32] M. A. Ordal, R. J. Bell, R. W. Alexander, L. L. J. Long, and M. R. Querry, Appl. Opt. **24**, 4493 (1985).
[33] W. J. Hillegas and J. B. Wagner, Bull. Am. Phys. Soc. **14**, 353 (1969).
[34] E. Gartstein, T. O. Mason, and J. B. Cohen, J. Phys. Chem. Solids **47**, 759 (1986).
[35] B. Szigeti, Proc. R. Soc London Ser. A **204**, 51 (1950).
[36] T. H. K. Barron and A. Batana, Philos. Mag. **20**, 619 (1969).
[37] H. K. Mao, T. Takahash, W. A. Bassett, and J. S. Weaver, J. Geophys. Res. **74**, 1061 (1969).
[38] B. Szigeti, Trans. Faraday Soc. **45**, 155 (1949).
[39] V. G. Baonza, M. Taravillo, M. Caceres, and J. Nunez, Phys. Rev. B **73**, 214117 (2006).
[40] M. P. Madan, Physica **51**, 526 (1971).
[41] A. V. Singh, J. C. Sharma, and J. Shanker, Physica B+C **94**, 331 (1978).